Correspondence

Frequency-Domain-Equalization-Aided Iterative Detection of Faster-Than-Nyquist Signaling

Shinya Sugiura, *Senior Member, IEEE*, and Lajos Hanzo, *Fellow, IEEE*

***Abstract*—A reduced-complexity three-stage-concatenated faster-than-Nyquist signaling (FTNS)-based transceiver architecture is proposed, which operates with the aid of soft decision (SoD) frequency-domain equalization (FDE) at the receiver. More specifically, the decoding algorithm conceived allows us to attain near-capacity performance as an explicit benefit of iterative detection, which is capable of eliminating the intersymbol interference imposed by FTNS. The proposed SoD FDE-aided FTNS detector has low decoding complexity that linearly increases upon increasing the FTNS block length and, hence, is particularly beneficial for practical long-dispersion scenarios. Furthermore, extrinsic information transfer charts are utilized for designing a near-capacity three-stage-concatenated turbo FTNS system, which exhibits an explicit turbo cliff in the low-signal-to-noise-ratio region, hence outperforming its conventional two-stage-concatenated FTNS counterpart.**

***Index Terms*—Extrinsic information transfer (EXIT) chart, faster-than-Nyquist signaling (FTNS), frequency-domain equalization (FDE), iterative detection, single-carrier transmission, soft-output detection, turbo coding.**

I. Introduction

The faster-than-Nyquist signaling (FTNS) concept enjoys its renaissance [1][1], although it was initially discovered by Mazo [2] as early as 1975. This is because the FTNS scheme is capable of increasing the transmission rate without increasing either the bandwidth or the number of transmit antennas. More specifically, in FTNS, more modulated symbols are transmitted in a given time window than in the classic time-orthogonal scenario obeying the Nyquist criterion, when assuming the same pulse shape, i.e., the same bandwidth. This implies that the FTNS scheme's symbol interval T is smaller than T_0 defined by the Nyquist criterion. As mentioned in [3], the rate-enhancement effect of FTNS may be as high as 30%–100%. Moreover, FTNS was extended to the family of nonbinary constellations [4] and multiple-input multiple-output (MIMO) contexts [5] for the sake of further exploiting the design degree of freedom.

Naturally, this is achieved at the cost of tolerating an increased ISI, which imposes an additional equalization burden on the FTNS receiver. In an uncoded high-rate FTNS scenario associated with a low interval ratio of $\alpha = T/T_0$ (i.e., a high-FTNS-rate scenario), the achievable bit error ratio (BER) performance is severely degraded by the detrimental effects of ISI. For example, in the FTNS scheme employing a sinc signaling pulse and binary phase-shift keying (BPSK) modulation, the optimal maximum likelihood (ML) receiver suffers from a performance penalty over its classic Nyquist-criterion-based counterpart, when the interval ratio α is lower than 0.802 [2].

To mitigate this limitation, it is beneficial to employ powerful channel codes [6] and [7], such as turbo and low-density parity-check codes. This beneficial performance improvement is reminiscent of that in rank-deficient MIMO arrangements [8] and [9], where interchannel interference is removed owing to the channel-decoder's iterative gain. The known iterative-detection-aided FTNS systems typically employ a two-stage serially concatenated turbo structure [6] and [10]. As a convenient design tool, extrinsic information transfer (EXIT) charts [11] and [12] have been conceived for analyzing the convergence behavior of the two-stage FTNS receiver's iterative detection [13]–[15]. To support iterative detection, the FTNS demodulator has to calculate both the soft decision (SoD) outputs from the received signals and soft *a priori* information from the SoD channel decoder's output. Since the main challenge of FTNS is high complexity, it is of paramount importance to develop a reduced-complexity SoD FTNS receiver algorithm. In [14], sphere decoding was invoked for FTNS, where the receiver had up to ten equalizer weights. In [16], the M-algorithm-aided BCJR (M-BCJR) decoder was proposed, which exhibits complexity reduction over both the reduced-trellis Viterbi algorithm and the BCJR benchmarkers. However, the aforementioned time-domain equalization (TDE)-based demodulators are unsuitable for high-memory FTNS equalization owing to its potentially excessive complexity.

To provide further insights, the aforementioned SoD FTNS decoding algorithms were developed under the simplifying assumptions of either additive white Gaussian noise (AWGN) or frequency-flat fading scenarios. However, when considering a highly dispersive frequency-selective gigabit scenario, having a channel impulse response (CIR) spreading over dozens or hundreds of short-duration symbols, the complexity may become prohibitive. Furthermore, having an α times lower symbol spacing than the Nyquist spacing results in a $1/\alpha$ times higher delay spread than that of its Nyquist-criterion-based counterpart. The same holds true in a guard-interval-assisted orthogonal frequency-division multiplexing FTNS scenario.

Most recently, in [17], the frequency-domain equalization (FDE) technique [18] that was originally developed for single-carrier frequency-division multiplexing access was applied to an uncoded hard-decision-based FTNS receiver for the first time. Owing to the explicit benefit of efficient fast Fourier transform (FFT)-based reception, this FDE receiver allows us to handle CIR spreading over thousands of symbols, while maintaining a realistic equalization complexity at the receiver. Unfortunately, this uncoded FDE-aided FTNS receiver fails to approach the optimal ML performance.

Against this background, the novel contributions of this paper are as follows.

1) Motivated by both the limitations and benefits of the recent FDE-aided hard-decision FTNS algorithm [17], we conceive a

Manuscript received December 28, 2013; revised March 26, 2014 and May 14, 2014; accepted July 6, 2014. This work was supported in part by the JST-ASTEP and in part by the Japan Society for the Promotion of Science KAKENHI under Grant 26630170. The review of this paper was coordinated by Prof. S.-H. Leung.

S. Sugiura is with the Department of Computer and Information Sciences, Tokyo University of Agriculture and Technology, Tokyo 183-8538, Japan (e-mail: sugiura@ieee.org).

L. Hanzo is with the School of Electronics and Computer Science, University of Southampton, Southampton SO17 1BJ, U.K. (e-mail: lh@ecs.soton.ac.uk).

Color versions of one or more of the figures in this paper are available online at http://ieeexplore.ieee.org.

Digital Object Identifier 10.1109/TVT.2014.2336984

[1]To expound a little further, the terminology of FTNS does not indicate a violation of Nyquist's sampling theorem. Rather, it is implied by FTNS that provided the employment of a specific band-limiting shaping pulse, such as a root raised cosine (RRC) filter, the symbol interval defined by the intersymbol interference (ISI)-free time-orthogonal Nyquist criterion is reduced so as to achieve a higher transmission rate. However, this achievement is at the cost of allowing the resultant ISI at the receiver.

low-complexity FDE-aided SoD demodulator for the FTNS receiver, which allows us to eliminate the ISI imposed by FTNS. The proposed scheme's low complexity is retained even in long-CIR scenarios.
2) Furthermore, we propose an advanced three-stage-concatenated FTNS transceiver, which is capable of attaining an infinitesimally low BER at a signal-to-noise ratio (SNR) close to the capacity bound.
3) Finally, we determine the maximum achievable rate, which is calculated based on EXIT charts.[2]

The remainder of this paper is organized as follows. In Section II, we detail our FTNS model and then introduce our three-stage-concatenated transceiver structure. Section III highlights our EXIT-chart-aided analysis and optimization, whereas the achievable error-rate performance is investigated in Section IV. Finally, we conclude in Section V.

II. System Model

Here, we first detail the system model of our cyclic prefix (CP)-assisted FTNS scheme, and then, the SoD FDE-aided demodulator is proposed. Finally, our serially concatenated three-stage FDE-aided FTNS transceiver structure is presented.

A. FTNS Modulation

Consider that a B-bit information sequence $\mathbf{b} = [b_1, \ldots, b_B] \in \mathbb{Z}^B$ is first mapped to N complex-valued symbols $\mathbf{s} = [s_1, \ldots, s_N]^T \in \mathbb{C}^N$. Then, a 2ν-sample CP $\mathbf{s}_{\rm cp} = [s_1, \ldots, s_{2\nu}]^T \in \mathbb{C}^{2\nu}$ is concatenated to the original symbol sequence $\mathbf{s}$ to construct $\bar{\mathbf{s}} = [\bar{s}_1, \ldots, \bar{s}_{N+2\nu}]^T = [\mathbf{s}^T, \mathbf{s}_{\rm cp}^T]^T \in \mathbb{C}^{N+2\nu}$. Finally, after each symbol has been convolved with the shaping pulse $h(t)$, the CP is inserted, and then, the signal is transmitted from a single transmit antenna using the symbol interval $T \leq T_0$.

At the receiver, the corresponding continuous-time received signals, which are matched-filtered by $h(t)$, are represented by

$$y(t) = \sum_n \bar{s}_n g(t - nT) + \eta(t) \tag{1}$$

where we have $g(t) = \int h(\tau)h^*(\tau - t)d\tau$ and $\eta(\tau) = \int n(\tau)h^*(\tau - t)d\tau$. Here, we assumed that an RRC filter having the roll-off factor β represents $h(t)$. Furthermore, $n(t)$ represents a random variable that obeys the zero-mean complex-valued Gaussian distribution $\mathcal{CN}(0, N_0)$, where N_0 is the noise variance. Under the perfect-synchronization assumption between the transmitter and the receiver, the kth sample is expressed as

$$\bar{y}_k = y(kT) \tag{2}$$

$$= \sum_n \bar{s}_n g(kT - nT) + \eta(kT). \tag{3}$$

Furthermore, upon removing the first and the last ν samples from $\bar{y} = [\bar{y}_1, \ldots, \bar{y}_{N+2\nu}]^T$, we arrive at the frequency-domain signal represented by [17]

$$\mathbf{y} = [\bar{y}_1, \ldots, \bar{y}_N]^T \in \mathbb{C}^N \tag{4}$$

$$= \mathbf{G}\mathbf{s} + \mathbf{n} \tag{5}$$

where $\mathbf{G}$ is a cyclic matrix, having the tap coefficient vector $\mathbf{g} = [g(-\nu T), \ldots, g(0), \ldots, g(\nu T)]^T \in \mathbb{R}^{2\nu+1}$, whereas $\mathbf{n}$ denotes the associated noise components. Note that similar to the assumption employed in [16], we consider the square norm $\|\mathbf{g}\|^2 = \mathbf{g}^H\mathbf{g}$ to be normalized to unity to ensure that the average received power per symbol be maintained at unity.

Here, it is assumed in (5) that the FTNS system's ISI tap length $L_{\rm FTN}$ in the AWGN channel is lower than the CP length ν and that other ISI components are truncated in this model. Note that in most of the previous FTNS studies, a similar truncation of high-tap terms is utilized. The exclusive benefit of our FDE-based approach is that the employment of a sufficiently high transmit-block length N makes the relative CP overhead $2\nu/N$ negligible.

B. SoD FDE-Based FTNS Detection

Let us now introduce the FDE-aided SoD FTNS demodulator, while assuming that BPSK modulation is employed for the sake of simplicity and of space economy. However, the extension to other nonbinary multilevel modulation schemes is readily applicable, similar to [4].

First, according to the soft-interference cancelation principle [21], the received signals are modified to

$$\tilde{\mathbf{y}} = \mathbf{y} - \mathbf{G}\tilde{\mathbf{s}} \tag{6}$$

$$= \mathbf{G}(\mathbf{s} - \tilde{\mathbf{s}}) + \mathbf{n} \tag{7}$$

where the soft symbols $\tilde{\mathbf{s}} = [\tilde{s}_1, \ldots, \tilde{s}_N]^T \in \mathbb{C}^N$ are generated from the *a priori* information, which is fed back from the outer decoder. Recalling that $\mathbf{G}$ is a circulant matrix, we can rely on FFT-assisted eigenvalue decomposition, which is formulated by [17]

$$\mathbf{G} = \mathbf{Q}^T \mathbf{\Lambda} \mathbf{Q}^* \tag{8}$$

where $\mathbf{Q}$ is the Fourier matrix defined by $[\mathbf{Q}]_{k.l} = (1/\sqrt{N}) \exp[-2\pi j(k-1)(l-1)/N]$. Furthermore, $\mathbf{\Lambda}$ is the diagonal matrix, whose ith element λ_i is the associated FFT coefficient. Hence, by carrying out the FFT operation on both sides of (7), we arrive at

$$\tilde{\mathbf{y}}_f = [\tilde{y}_{f,1}, \ldots, \tilde{y}_{f,N}]^T \tag{9}$$

$$= \mathbf{Q}^* \tilde{\mathbf{y}} \tag{10}$$

$$= \mathbf{\Lambda}\mathbf{Q}^*(\mathbf{s} - \tilde{\mathbf{s}}) + \mathbf{n}_f \in \mathbb{C}^N \tag{11}$$

where $\mathbf{n}_f = \mathbf{Q}^*\mathbf{n}$ is the associated noise vector.

With the aid of minimum mean square error (MMSE) filtering, the frequency-domain symbol estimates $\hat{\mathbf{s}}_f = [\hat{s}_{f,1}, \ldots, \hat{s}_{f,N}]^T \in \mathbb{C}^N$ are given by [22]

$$\hat{s}_{f,n} = \frac{\lambda_i^*}{|\lambda_n|^2 D + N_0} \tilde{y}_{f,n} \tag{12}$$

where we have

$$D = -\sum_{i=1}^{N} |\tilde{s}_i|^2 / N. \tag{13}$$

Finally, the time-domain extrinsic log-likelihood ratio (LLR) outputs of the proposed demodulator are formulated as follows [23]:

$$\mathbf{L}_{\rm e} = [L_{\rm e}(b_1), \ldots, L_{\rm e}(b_N)]^T \tag{14}$$

$$= \frac{\gamma\tilde{\mathbf{s}} + \mathbf{Q}^T\hat{\mathbf{s}_f}}{1 + \gamma\delta} \in \mathbb{R}^N \tag{15}$$

[2]To elaborate a little further, the maximum achievable rate represents the maximum practically attainable rate that takes into account the effects of a specific inner code, modulation and detection scheme, unlike the classic capacity bound. Hence, it is possible to appropriately characterize the proposed reduced-complexity SoD detector. For a detailed discussion, please refer to [19] and [20].

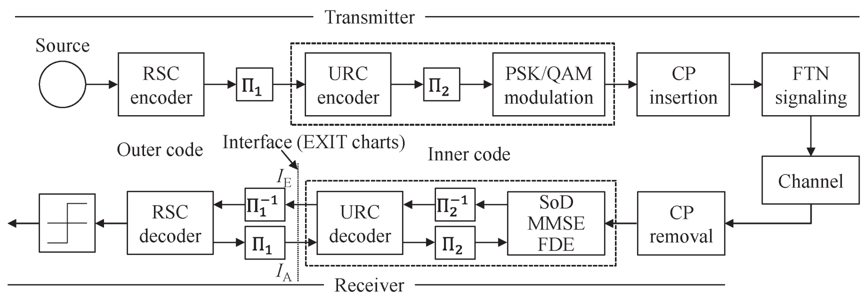

Fig. 1. Transmitter and receiver structures of our FTNS-based three-stage serially concatenated system.

where

$$\gamma = \Re\left[\sum_{i=1}^{N} \frac{|\lambda_i|^2/\left(|\lambda_i|^2 D + N_0\right)}{N}\right] \tag{16}$$

$$\delta = 1 - D. \tag{17}$$

Although in the derivation of our SoD FDE-aided FTNS demodulator we assumed having an AWGN channel, the proposed SoD demodulator is readily applicable to either frequency-flat or frequency-selective fading scenarios, provided that we set the CP size sufficiently high, as shown in [17].

C. Extension to the Frequency-Selective Fading System Model

Having introduced our FTNS transceiver model under a simplified AWGN channel assumption, let us now consider its extension to a model applicable to frequency-selective fading environments. Let us consider that the delay spread associated with frequency-selective channels spans over $L_{\mathrm{DS}}T(=\alpha L_{\mathrm{DS}}T_0)$ symbol durations and that the L_{DS} complex-valued tap coefficients are given by q_l $(l = 0, \ldots, L_{\mathrm{DS}}-1)$. Then, by defining the first term of (3) as

$$\bar{y}_k = \sum_{n=-\nu}^{\nu} \bar{s}_n g(kT - nT) \tag{18}$$

the received signal may be expressed as

$$y_k = \sum_{l=0}^{L_{\mathrm{DS}}-1} q_l \bar{y}_{k-l} + \eta(kT) \tag{19}$$

$$= \sqrt{E_s} \sum_{l=0}^{L_{\mathrm{DS}}-1} \sum_{n=-\nu}^{\nu} s_n q_l g\left(kT - (l+n)T\right) + \eta(kT). \tag{20}$$

This system model also represents a circular-matrix-based linear block structure in the same manner as $\mathbf{G}$ of (5), where the CP length of 2ν is designed to be sufficiently higher than the effective ISI duration. Therefore, the FDE-aided FTNS technique derived in Section II-B is also readily applicable in this frequency-selective scenario.

Note that the effective ISI length in the frequency-selective scenario is a factor $(L_{\mathrm{DS}}-1)$ higher than that considered for its frequency-flat FTNS counterpart in Section II-B. Furthermore, when we compare the effective CIR length of the FTNS- and Nyquist-sampled scenarios, the ratio becomes

$$\theta = \frac{L_{\mathrm{DS}} + L_{\mathrm{FTN}}}{\alpha L_{\mathrm{DS}}} \tag{21}$$

implying that a lower α value corresponds to a wider gap between the two. Naturally, this typically increases the detection complexity; hence, the advantage of the proposed low-complexity FDE-aided FTNS receiver over its conventional time-domain counterpart becomes further improved in this practical scenario.

D. Three-Stage-Concatenated FTNS System

Having introduced the SoD FDE-aided FTNS demodulator in Section II-B, we further improve it with the aid of a multistage serially concatenated turbo FTNS architecture, to achieve a near-capacity performance, while eliminating the limitations of ISI. More specifically, we propose the three-stage-concatenated recursive systematic convolutional (RSC)-encoded and unity-rate convolutional (URC)-encoded transmitter structure in Fig. 1. At the transmitter, the information bits are first encoded by the RSC encoder, and then, the encoded bits are interleaved by the first interleaver Π_1. Next, the interleaved bits are URC-encoded and then interleaved again by the second interleaver Π_2. Finally, the interleaved bits are mapped by the CP-assisted low-complexity FTNS modulator described in Section II-A, to construct the $(N+2\nu)$-symbol sequence to be transmitted.

As shown in Fig. 1, a three-stage iterative decoding algorithm is employed at the receiver. To be specific, the SoD decoders of the receiver iteratively exchange soft extrinsic information in the form of LLRs. The SoD MMSE FDE block in Fig. 1 receives its input signals after CP removal, which are combined with the extrinsic information provided by the URC decoder. Simultaneously, the URC decoder block in Fig. 1 receives extrinsic information from both the RSC channel decoder and the SoD MMSE FDE demodulator and generates extrinsic information for both of its surrounding blocks, as shown in Fig. 1. The RSC channel decoder in Fig. 1 exchanges extrinsic information with the URC decoder and outputs the estimated bits after I_{out} iterations. Here, the iterations between the SoD MMSE FDE and URC decoder blocks are referred to as the inner iterations, whereas those between the URC and RSC decoders are referred to as outer iterations. The number of these iterations is represented by I_{in} and I_{out}, respectively. To be more specific, I_{in} inner iterations are implemented per each outer iteration, indicating that the total number of iterations is $I_{\mathrm{in}} \cdot I_{\mathrm{out}}$. Hence, when fixing the number of inner iterations I_{in}, it becomes possible to rely on the 2-D projection of the associated 3-D EXIT charts [19].[3]

[3]To exactly estimate the convergence behavior of our three-stage-concatenated iterative receiver, ideally, 3-D EXIT charts [24] would be used. However, they impose high analysis complexity. By contrast, the projection to 2-D EXIT charts allows us to efficiently analyze the associated iterative behavior, when the number of inner iterations I_{in} is sufficiently high for approaching the highest possible mutual information between the inner blocks [19]. Furthermore, this makes it easier to compare the iterative behaviors of the two-stage- and three-stage-concatenated iterative receivers, as demonstrated in Section III.

III. EXIT-Chart-Aided Optimization

Here, we analyze the convergence behavior of our multistage-concatenated FTNS systems. Here, we invoke EXIT charts for characterizing the FTNS scheme's near-capacity code design and the information-theoretic analysis of the maximum achievable rate.

A. Semianalytical Evaluations of Maximum Achievable Rate

In turbo detection, an infinitesimally low BER may be attained by the iterative exchange of extrinsic mutual information between multiple SoD decoders. Since the iterative decoding process is nonlinear, the prediction of its convergence behavior is a challenging task. The ingenious tool of EXIT charts was proposed by ten Brink [12] for both the visualization of the iterative decoding behavior and for the prediction of the "BER-cliff"-SNR position, where the BER suddenly drops. More specifically, the input/output relationship of the mutual information at each decoder is characterized by the EXIT chart, and then, their interaction assisted by the iterative decoding process is examined without time-consuming bit-by-bit Monte Carlo simulations.

The explicit benefit of utilizing EXIT charts for the analysis of FTNS is the capability of evaluating arbitrary detectors, including suboptimal detectors. As previously mentioned, the SoD maximum *a posteriori* (MAP) detection, which has been typically considered for the conventional channel-encoded FTNS scheme, exhibits excessive decoding complexity. Furthermore, deriving the exact performance bound of a suboptimal FTNS detector is a challenging task.

By exploiting the EXIT chart's area property detailed in [19], let us define the maximum achievable rate of our FDE-aided FTNS system as

$$\mathcal{C}_{\mathrm{EXIT}} = \frac{N}{N+2\nu} \cdot \frac{\log_2 \mathcal{M}}{\alpha(1+\beta)} \cdot \mathcal{A}(\rho) \tag{22}$$

where $\mathcal{A}(\rho)$ represents the area under the inner code's EXIT curve at SNR $= \rho$. To be more specific, when assuming that the area under an outer code's EXIT curve is perfectly matched to that under an inner code's EXIT curve, the maximum achievable rate of a serially concatenated scheme may be approximated by evaluating the area under the EXIT curves, as detailed in [19] and [25]. Exploiting this EXIT-chart-based limit allows us to evaluate the maximum attainable rate of an arbitrary iterative FTNS detection algorithm.

B. EXIT-Chart-Based Analysis of FTNS

Here, we investigate the convergence behavior and the maximum achievable rate of some specific FTNS scenarios. Here, the input/output interface of EXIT charts was assumed to be positioned between the first interleaver Π_1 and the inner code, as shown in Fig. 1. Furthermore, in addition to our three-stage-concatenated FTNS system, we also considered its two-stage counterpart as our benchmark scheme, where the second interleaver Π_2/deinterleaver Π_2^{-1} and the URC encoder/decoder were removed from the architecture in Fig. 1. In Fig. 2, we plotted the EXIT charts of our FDE-aided two-stage FTNS system, employing BPSK modulation and the FTNS parameters of $(\alpha, \beta, \nu) = (0.6, 0.5, 10)$, where the SNR was varied from -5 to 2 dB with steps of 1 dB. We also plotted the inner code's EXIT curves associated with classic Nyquist signaling. The half-rate unit-memory RSC(2,1,2) code, having the octally represented generator polynomial of $(G_r, G) = (3, 2)$ [11], was employed for the outer code, where G_r stands for the recursive feedback polynomial and feedforward polynomial G. Further, a simple rate-one accumulator, represented by the generator polynomials (3,2) expressed in octal form, was considered for the URC precoder. Observe in Fig. 2 that regardless of the SNR value, our two-stage FDE-based FTNS system converged to that of its classic Nyquist-criterion-based counterpart for $I_{\mathrm{A}} = 1.0$. Hence, it is predicted that our proposed low-complexity FDE-based algorithm is capable of achieving the same error-rate performance as that of the equivalent Nyquist-criterion-based scheme, which is an explicit benefit of the iterative receiver architecture.[4]

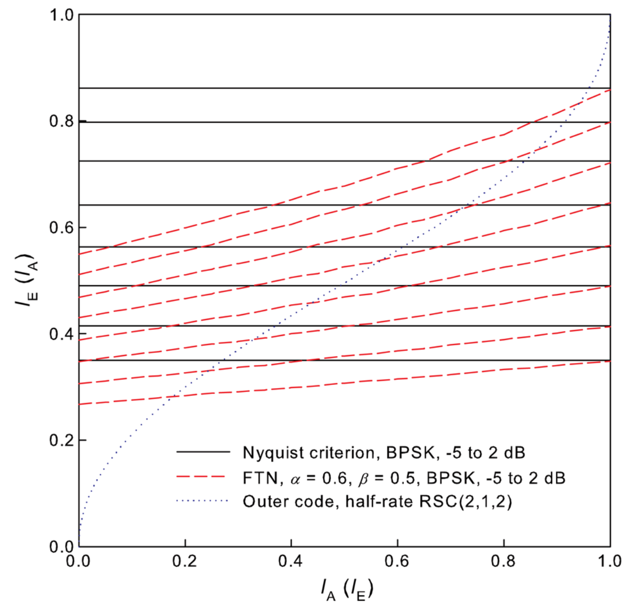

Fig. 2. EXIT charts of our FDE-aided two-stage FTNS system, employing the BPSK modulation and FTNS parameters of $(\alpha, \beta, \nu) = (0.6, 0.5, 10)$, where the SNR was varied from -5 to 2 dB with steps of 1 dB. The number of inner iterations was maintained to be $I_{\mathrm{in}} = 2$ throughout this paper. Moreover, we plotted the inner code's EXIT curves associated with the classic Nyquist-criterion scenario, while showing the outer code's EXIT curve corresponding to the half-rate RSC(2,1,2) code, having the generator polynomial of $(G_r, G) = (3, 2)$.

In Fig. 3, we drew the EXIT charts of our FDE-aided three-stage FTNS system, employing BPSK modulation and the FTNS parameters of $(\alpha, \beta, \nu) = (0.6, 0.5, 10)$, where the SNR was set to 1 dB. We also plotted the inner code's EXIT curves associated with the conventional Nyquist criterion, while showing the outer code's EXIT curve corresponding to the half-rate RSC(2,1,2) code, having the octal generator polynomials of (3,2). The transmit block length was set to $N = 2^{17}$. It can be seen in Fig. 3 that our three-stage FTNS scheme approached the point $(I_{\mathrm{A}}, I_{\mathrm{E}}) = (1.0, 1.0)$ of perfect convergence to an infinitesimally low BER. This was achieved as the explicit benefit of the URC precoder, which creates an infinite impulse response inner decoder component [27] and [28] to reach the $(I_{\mathrm{A}}, I_{\mathrm{E}}) = (1, 1)$ point of convergence in the EXIT chart, hence achieving an infinitesimally low BER.

This was also confirmed by the Monte-Carlo-simulation-based EXIT trajectory shown in Fig. 3.

Furthermore, in Fig. 4, we plotted the EXIT charts of our three-stage-concatenated FDE-aided FTNS systems, where the roll-off factor β was given by (a) 0.1, (b) 0.5, while maintaining the symbol's packing ratio of $\alpha = 0.6$. The SNR of the outer code's EXIT curve was varied from -10 to 10 dB with steps of 1 dB. It can be seen in Fig. 4 that at high SNRs, a higher-β inner-code EXIT curve corresponds to

[4]To provide further insights, this inner code's convergence to that of its interference-free Nyquist-criterion-based counterpart can also be seen in rank-deficient spatial-multiplexing MIMO scenarios [26], where the number of receive antenna elements is lower than that of the transmit antenna elements.

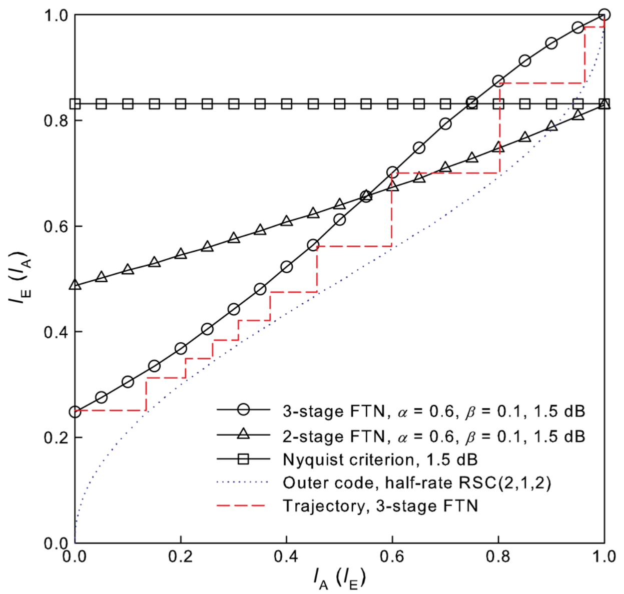

Fig. 3. EXIT charts of our FDE-aided three-stage FTNS system, employing BPSK modulation and the FTNS parameters of $(\alpha, \beta, \nu) = (0.6, 0.5, 10)$, where the SNR was set to 1 dB. Moreover, we plotted the inner code's EXIT curves associated with the classic Nyquist-criterion scenario, while showing the outer code's EXIT curve corresponding to the half-rate RSC(2,1,2) code, which has the generator polynomial (3,2). The code length was set to $N = 2^{17}$.

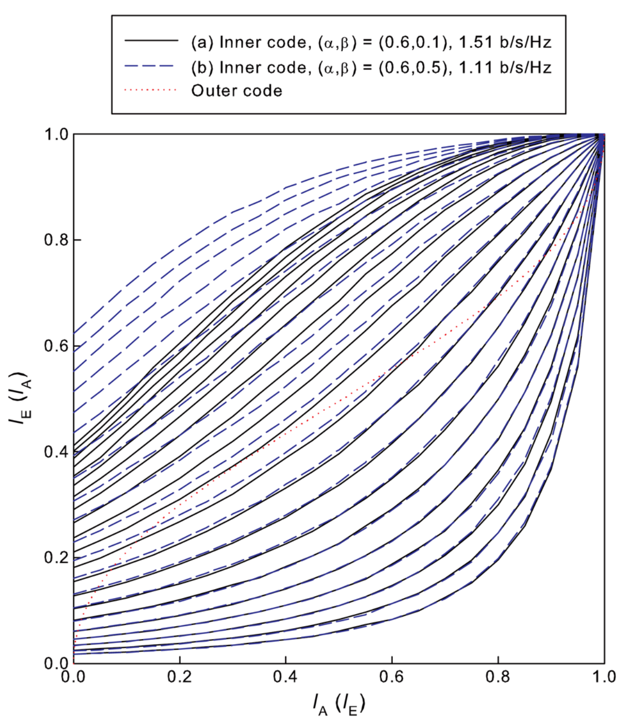

Fig. 4. EXIT charts of our three-stage-concatenated FDE-aided FTNS systems, where the roll-off factor β was given by (a) 0.1, (b) 0.5, while maintaining the symbol's packing ratio $\alpha = 0.6$. The SNR of the outer code's EXIT curve was varied from -10 to 10 dB with steps of 1 dB.

a higher performance, i.e., to a wider open-tunnel area between the inner and outer codes' EXIT curves. However, regardless of the roll-off factor value β, an open EXIT tunnel emerged at SNR ≥ 1 dB; therefore, affording an increased number of iterations enabled us to attain a higher transmission rate without imposing any SNR penalty,

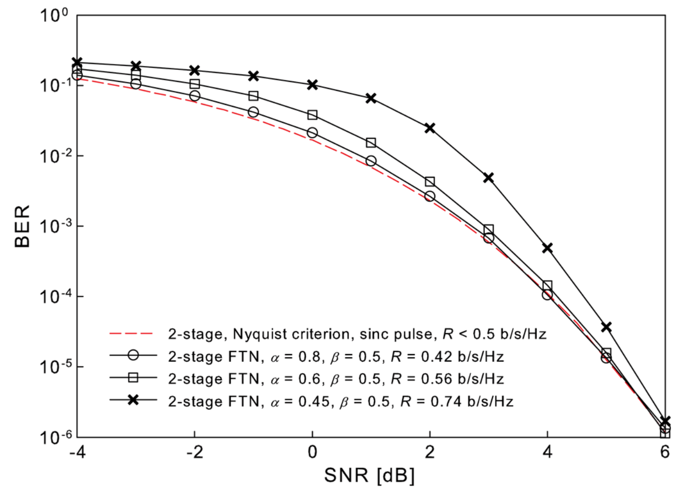

Fig. 5. Achievable BER of our FDE-aided two-stage RSC-encoded FTNS systems, employing BPSK modulation and FTNS parameters of $(\alpha, \beta, \nu) = (0.45, 0.5, 10)$, (0.6, 0.5, 10), and (0.8, 0.5, 10). Moreover, we plotted the BER curve of the conventional Nyquist-criterion scenario as a benchmark scheme. The half-rate RSC(2,1,2) code, having the polynomial generator of (3,2) and the code length $N = 2^{17}$, was considered.

which is particularly beneficial for our FTNS receiver exhibiting low detection complexity.[5]

As previously mentioned, nonbinary multilevel modulation schemes may also be used for our FTNS scheme instead of a binary modulation scheme. However, in such a scenario, either the bitwise soft-input/output relationship has to be considered for the EXIT chart analysis, as shown in [23], or corresponding symbol-based EXIT charts have to be used.

IV. Error-Rate Performance Results

To further characterize our FDE-aided two- and three-stage-concatenated FTNS systems, we investigated their BER based on extensive Monte Carlo simulations.

First, Fig. 5 shows the achievable BER of our FDE-aided two-stage FTNS systems employing BPSK modulation and FTNS parameters of $(\alpha, \beta, \nu) = (0.45, 0.5, 10)$, (0.6, 0.5, 10), and (0.8, 0.5, 10), along with the BER of the conventional Nyquist-criterion-based scenario as a benchmarker and with the outer code's EXIT curve corresponding to the half-rate RSC(2,1,2) code, having the octal generator polynomials of (3,2). The transmit block length was set to $N = 2^{17}$. In this simulation scenario, our FTNS scheme's transmission rate was varied from 0.42 to 0.74 b/s/Hz, while, at the same time, the symbol packing coefficient α was decreased from 0.8 to 0.45. Observe in Fig. 5 that the two-stage iterative detection converged to the ISI-free Nyquist-criterion-based curve upon increasing SNR. This was achieved regardless of the symbol packing ratio α. More specifically, this configured the EXIT chart analysis conducted in Fig. 2. Observe that our reduced-complexity FDE receiver was found to perfectly eliminate the ISI effects, similar to its time-domain SoD MAP counterparts characterized [6] and [1].

In Fig. 6, we compared the achievable BER curves of our FDE-aided two- and three-stage FTNS systems employing BPSK modulation and

[5] In the simulations, we only considered the half-rate RSC(2,1,2) code as our outer code. However, it may be possible to employ other types of outer codes, which potentially attains a better match between the outer and inner codes' EXIT curves. For example, irregular channel codes [19] and [24] are capable of flexibly designing an outer code's EXIT curve, which matches the inner code's EXIT curve at a given SNR.

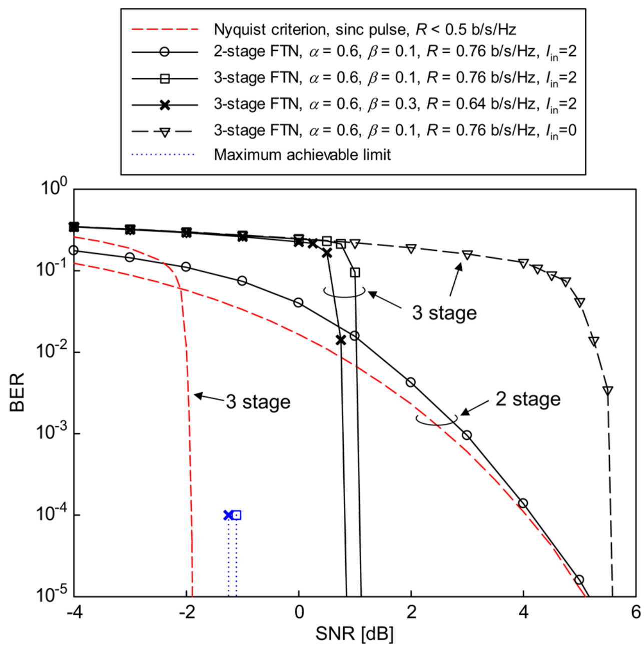

Fig. 6. Achievable BER of our FDE-aided two- and three-stage FTNS systems, employing BPSK modulation and FTNS parameter sets of $(\alpha, \beta, \nu) = (0.6, 0.1, 10)$ and (0.6, 0.3, 10). Moreover, we plotted the BER of the conventional Nyquist-criterion scenario. Here, we assumed the employment of the half-rate RSC(2,1,2) code, which has the polynomial generator (3,2) and a code length $N = 2^{17}$.

the FTNS parameter sets of $(\alpha, \beta, \nu) = (0.6, 0.1, 10)$ and (0.6, 0.3, 10). We also plotted the two BER curves associated with the conventional Nyquist-criterion-based scenario. Moreover, we plotted the associated BER curve of the FDE-aided three-stage FTNS system that dispenses with inner iterations, i.e., for $I_{\rm in} = 0$, to explicitly clarify the beneficial effects of the *a priori* information fed back to our SoD FDE. Here, we assumed the employment of the half-rate RSC(2,1,2) code, having the octal generator polynomials of (3,2), and the block length was set to $N = 2^{17}$. It was found in Fig. 6 that both the proposed three-stage systems having $\beta = 0.1$ and 0.3 exhibited an infinitesimally low BER at SNR $= 1.0$ and 1.3 dB, respectively, whereas its two-stage counterpart did not. More specifically, these BER cliffs were apart by as little as 2.1 and 2.5 dB from the maximum achievable limits, which were calculated based on the EXIT chart analysis in Fig. 3. Note that the BER curves of the Nyquist-criterion-based systems were calculated under the idealistic assumption of sinc-pulse transmissions, which cannot be used in a practical system. Additionally, the transmission rate was lower than that of the FTNS systems. Moreover, the three-stage FTNS system dispensing with inner iterations ($I_{\rm in} = 0$) imposed more than 4-dB performance penalty in comparison to that having $I_{\rm in} = 2$ inner iterations. Therefore, the joint optimization of the three SoD decoders is quite crucial for the sake of ensuring the most appropriate extrinsic-information exchange.

Finally, in Fig. 7, we plotted the BER curves of our three-stage-concatenated FTNS systems having the CP length of $2\nu = 32$, 36, 40, and 48, when using a constant block length of 512 bits, while considering frequency-selective block Rayleigh fading. Furthermore, the interleaver length of 2^{17} and the FTNS parameter set of $(\alpha, \beta) = (0.6, 0.1)$ were employed. The delay spread was set to $L_{\rm DS} = 20$. Furthermore, the fading coefficients q_l $(l = 0, \ldots, L_{\rm DS})$ were randomly generated according to the complex-valued Gaussian distribution $\mathcal{CN}(0,1/L_{\rm DS})$. Observe in Fig. 7 that upon increasing the CP length, the error floor caused by the FTNS-induced ISI and by the

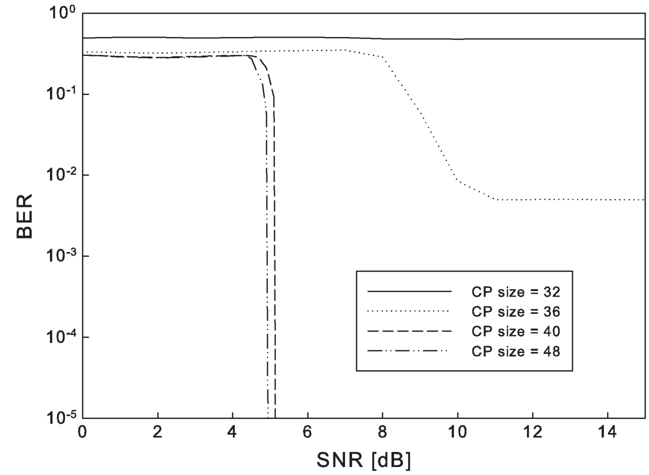

Fig. 7. Achievable BER of our FDE-aided three-stage FTNS systems, experiencing frequency-selective block Rayleigh fading, where we considered the delay spread of $L_{\rm DS} = 20$ taps. The BPSK modulation and the FTNS parameter set of $(\alpha, \beta) = (0.6, 0.1)$ were employed, while varying the CP length 2ν from 32 to 48. Here, we assumed the employment of the half-rate RSC(2,1,2) code, which has the polynomial generator (3,2) and a code length $N = 2^{17}$.

long-CIR dispersive channel was eliminated. More specifically, it was found that to compensate the ISI, a CP length of $2\nu \geq 40$ was required in this specific simulation scenario. This implies that the conventional TDE-based FTNS receivers are incapable of supporting such a long CIR owing to their prohibitively high decoding complexity.

V. Conclusion

In this paper, we have proposed a novel reduced-complexity SoD FTNS receiver structure for long-CIR gigabit systems, which relied on the FDE principle. The proposed detector is capable of eliminating FTNS-specific ISI, while maintaining practical decoding complexity. Furthermore, we carried out its comprehensive EXIT-chart-aided analysis to design a near-capacity three-stage serially concatenated FTNS architecture, which is free from an error floor. Our simulation results demonstrated that the proposed FTNS scheme has the explicit benefits of lower complexity and better BER performance than those of its conventional channel-encoded FTNS counterpart.

References

[1] J. B. Anderson, F. Rusek, and V. Owall, "Faster than Nyquist signaling," *Proc. IEEE*, vol. 101, no. 8, pp. 1817–1830, Aug. 2013.
[2] J. E. Mazo, "Faster-than-Nyquist signaling," *Bell Syst. Tech. J.*, vol. 54, no. 8, pp. 1451–1462, Oct. 1975.
[3] J. Esch, "Prolog to faster-than-Nyquist signaling," *Proc. IEEE*, vol. 101, no. 8, pp. 1815–1816, Aug. 2013.
[4] F. Rusek and J. B. Anderson, "Non binary and precoded faster than Nyquist signaling," *IEEE Trans. Commun.*, vol. 56, no. 5, pp. 808–817, May 2008.
[5] F. Rusek, "On the existence of the Mazo-limit on MIMO channels," *IEEE Trans. Wireless Commun.*, vol. 8, no. 3, pp. 1118–1121, Mar. 2009.
[6] A. D. Liveris and C. N. Georghiades, "Exploiting faster-than-Nyquist signaling," *IEEE Trans. Comm.*, vol. 51, no. 9, pp. 1502–1511, Sep. 2003.
[7] G. Colavolpe, T. Foggi, A. Modenini, and A. Piemontese, "Faster-than-Nyquist and beyond: How to improve spectral efficiency by accepting interference," *Opt. Exp.*, vol. 19, no. 27, pp. 26 600–26 609, Dec. 2011.
[8] S. Liu and Z. Tian, "Near-optimum soft decision equalization for frequency selective MIMO channels," *IEEE Trans. Signal Process.*, vol. 52, no. 3, pp. 721–733, Mar. 2004.
[9] S. Sugiura, S. Chen, and L. Hanzo, "MIMO-aided near-capacity turbo transceivers: Taxonomy and performance versus complexity," *IEEE Commun. Surveys Tuts.*, vol. 14, no. 2, pp. 421–442, 2012.

[10] F. Rusek and J. Anderson, "Multistream faster than Nyquist signaling," *IEEE Trans. Commun.*, vol. 57, no. 5, pp. 1329–1340, May 2009.

[11] S. ten Brink, "Designing iterative decoding schemes with the extrinsic information transfer chart," *AEU Int. J. Electron. Commun.*, vol. 54, no. 6, pp. 389–398, Nov. 2000.

[12] S. ten Brink, "Convergence behavior of iteratively decoded parallel concatenated codes," *IEEE Trans. Commun.*, vol. 49, no. 10, pp. 1727–1737, Oct. 2001.

[13] A. Prlja, J. B. Anderson, and F. Rusek, "Receivers for faster-than-Nyquist signaling with and without turbo equalization," in *Proc. IEEE Int. Symp. Inf. Theory*, Toronto, Canada, Jul. 6–11, 2008, pp. 464–468.

[14] M. McGuire and M. Sima, "Discrete time faster-than-Nyquist signalling," in *Proc. IEEE Global Telecommun. Conf.*, 2010, pp. 1–5.

[15] J. B. Anderson and M. Zeinali, "Best rate 1/2 convolutional codes for turbo equalization with severe ISI," in *Proc. IEEE ISIT*, 2012, pp. 2366–2370.

[16] A. Prlja and J. B. Anderson, "Reduced-complexity receivers for strongly narrowband intersymbol interference introduced by faster-than-Nyquist signaling," *IEEE Trans. Commun.*, vol. 60, no. 9, pp. 2591–2601, Sep. 2012.

[17] S. Sugiura, "Frequency-domain equalization of faster-than-Nyquist signaling," *IEEE Wireless Commun. Lett.*, vol. 2, no. 5, pp. 555–558, Oct. 2013.

[18] D. Falconer, S. Ariyavisitakul, A. Benyamin-Seeyar, and B. Eidson, "Frequency domain equalization for single-carrier broadband wireless systems," *IEEE Commun. Mag.*, vol. 40, no. 4, pp. 58–66, Apr. 2002.

[19] L. Hanzo, O. Alamri, M. El-Hajjar, and N. Wu, *Near-Capacity Multi-Functional MIMO Systems: Sphere-Packing, Iterative Detection and Cooperation*. Hoboken, NJ, USA: Wiley, 2009.

[20] M. El-Hajjar and L. Hanzo, "EXIT charts for system design and analysis," *IEEE Commun. Surveys Tuts.*, vol. 16, no. 1, pp. 127–153, 2014, early access in IEEE Xplore.

[21] M. Tüchler, A. Singer, and R. Koetter, "Minimum mean squared error equalization using *a priori* information," *IEEE Trans. Signal Process.*, vol. 50, no. 3, pp. 673–683, Mar. 2002.

[22] B. Ng, C.-T. Lam, and D. Falconer, "Turbo frequency domain equalization for single-carrier broadband wireless systems," *IEEE Trans. Wireless Commun.*, vol. 6, no. 2, pp. 759–767, Feb. 2007.

[23] K. Kansanen and T. Matsumoto, "An analytical method for MMSE MIMO turbo equalizer EXIT chart computation," *IEEE Trans. Wireless Commun.*, vol. 6, no. 1, pp. 59–63, Jan. 2007.

[24] F. Brännström, L. K. Rasmussen, and A. J. Grant, "Convergence analysis and optimal scheduling for multiple concatenated codes," *IEEE Trans. Inf. Theory*, vol. 51, no. 9, pp. 3354–3364, Sep. 2005.

[25] A. Ashikhmin, G. Kramer, and S. Ten Brink, "Extrinsic information transfer functions: Model and erasure channel properties," *IEEE Trans. Inf. Theory*, vol. 50, no. 11, pp. 2657–2673, Nov. 2004.

[26] L. Xu, S. Chen, and L. Hanzo, "EXIT chart analysis aided turbo MUD designs for the rank-deficient multiple antenna assisted OFDM uplink," *IEEE Trans. Wireless Communications*, vol. 7, no. 6, pp. 2039–2044, Jun. 2008.

[27] S. Benedetto, D. Divsalar, G. Montorsi, and F. Pollara, "Serial concatenation of interleaved codes: Performance analysis, design, iterative decoding," *IEEE Trans. Inf. Theory*, vol. 44, no. 3, pp. 909–926, May 1998.

[28] F. Schreckenbach and G. Bauch, "Bit-interleaved coded irregular modulation," *Eur. Trans. Telecommun.*, vol. 17, no. 2, pp. 269–282, Mar./Apr. 2006.

AUTHOR QUERIES

AUTHOR PLEASE ANSWER ALL QUERIES

AQ1 = Please provide the expanded forms of “JST-ASTEP” and “KAKENHI” if such are acronyms.

END OF ALL QUERIES

Correspondence

Frequency-Domain-Equalization-Aided Iterative Detection of Faster-Than-Nyquist Signaling

Shinya Sugiura, *Senior Member, IEEE*, and Lajos Hanzo, *Fellow, IEEE*

***Abstract*—A reduced-complexity three-stage-concatenated faster-than-Nyquist signaling (FTNS)-based transceiver architecture is proposed, which operates with the aid of soft decision (SoD) frequency-domain equalization (FDE) at the receiver. More specifically, the decoding algorithm conceived allows us to attain near-capacity performance as an explicit benefit of iterative detection, which is capable of eliminating the intersymbol interference imposed by FTNS. The proposed SoD FDE-aided FTNS detector has low decoding complexity that linearly increases upon increasing the FTNS block length and, hence, is particularly beneficial for practical long-dispersion scenarios. Furthermore, extrinsic information transfer charts are utilized for designing a near-capacity three-stage-concatenated turbo FTNS system, which exhibits an explicit turbo cliff in the low-signal-to-noise-ratio region, hence outperforming its conventional two-stage-concatenated FTNS counterpart.**

***Index Terms*—Extrinsic information transfer (EXIT) chart, faster-than-Nyquist signaling (FTNS), frequency-domain equalization (FDE), iterative detection, single-carrier transmission, soft-output detection, turbo coding.**

I. Introduction

The faster-than-Nyquist signaling (FTNS) concept enjoys its renaissance [1][1], although it was initially discovered by Mazo [2] as early as 1975. This is because the FTNS scheme is capable of increasing the transmission rate without increasing either the bandwidth or the number of transmit antennas. More specifically, in FTNS, more modulated symbols are transmitted in a given time window than in the classic time-orthogonal scenario obeying the Nyquist criterion, when assuming the same pulse shape, i.e., the same bandwidth. This implies that the FTNS scheme's symbol interval T is smaller than T_0 defined by the Nyquist criterion. As mentioned in [3], the rate-enhancement effect of FTNS may be as high as 30%–100%. Moreover, FTNS was extended to the family of nonbinary constellations [4] and multiple-input multiple-output (MIMO) contexts [5] for the sake of further exploiting the design degree of freedom.

Manuscript received December 28, 2013; revised March 26, 2014 and May 14, 2014; accepted July 6, 2014. This work was supported in part by the JST-ASTEP and in part by the Japan Society for the Promotion of Science KAKENHI under Grant 26630170. The review of this paper was coordinated by Prof. S.-H. Leung.

S. Sugiura is with the Department of Computer and Information Sciences, Tokyo University of Agriculture and Technology, Tokyo 183-8538, Japan (e-mail: sugiura@ieee.org).

L. Hanzo is with the School of Electronics and Computer Science, University of Southampton, Southampton SO17 1BJ, U.K. (e-mail: lh@ecs.soton.ac.uk).

Color versions of one or more of the figures in this paper are available online at http://ieeexplore.ieee.org.

Digital Object Identifier 10.1109/TVT.2014.2336984

[1]To expound a little further, the terminology of FTNS does not indicate a violation of Nyquist's sampling theorem. Rather, it is implied by FTNS that provided the employment of a specific band-limiting shaping pulse, such as a root raised cosine (RRC) filter, the symbol interval defined by the intersymbol interference (ISI)-free time-orthogonal Nyquist criterion is reduced so as to achieve a higher transmission rate. However, this achievement is at the cost of allowing the resultant ISI at the receiver.

Naturally, this is achieved at the cost of tolerating an increased ISI, which imposes an additional equalization burden on the FTNS receiver. In an uncoded high-rate FTNS scenario associated with a low interval ratio of $\alpha = T/T_0$ (i.e., a high-FTNS-rate scenario), the achievable bit error ratio (BER) performance is severely degraded by the detrimental effects of ISI. For example, in the FTNS scheme employing a sinc signaling pulse and binary phase-shift keying (BPSK) modulation, the optimal maximum likelihood (ML) receiver suffers from a performance penalty over its classic Nyquist-criterion-based counterpart, when the interval ratio α is lower than 0.802 [2].

To mitigate this limitation, it is beneficial to employ powerful channel codes [6] and [7], such as turbo and low-density parity-check codes. This beneficial performance improvement is reminiscent of that in rank-deficient MIMO arrangements [8] and [9], where interchannel interference is removed owing to the channel-decoder's iterative gain. The known iterative-detection-aided FTNS systems typically employ a two-stage serially concatenated turbo structure [6] and [10]. As a convenient design tool, extrinsic information transfer (EXIT) charts [11] and [12] have been conceived for analyzing the convergence behavior of the two-stage FTNS receiver's iterative detection [13]–[15]. To support iterative detection, the FTNS demodulator has to calculate both the soft decision (SoD) outputs from the received signals and soft *a priori* information from the SoD channel decoder's output. Since the main challenge of FTNS is high complexity, it is of paramount importance to develop a reduced-complexity SoD FTNS receiver algorithm. In [14], sphere decoding was invoked for FTNS, where the receiver had up to ten equalizer weights. In [16], the M-algorithm-aided BCJR (M-BCJR) decoder was proposed, which exhibits complexity reduction over both the reduced-trellis Viterbi algorithm and the BCJR benchmarkers. However, the aforementioned time-domain equalization (TDE)-based demodulators are unsuitable for high-memory FTNS equalization owing to its potentially excessive complexity.

To provide further insights, the aforementioned SoD FTNS decoding algorithms were developed under the simplifying assumptions of either additive white Gaussian noise (AWGN) or frequency-flat fading scenarios. However, when considering a highly dispersive frequency-selective gigabit scenario, having a channel impulse response (CIR) spreading over dozens or hundreds of short-duration symbols, the complexity may become prohibitive. Furthermore, having an α times lower symbol spacing than the Nyquist spacing results in a $1/\alpha$ times higher delay spread than that of its Nyquist-criterion-based counterpart. The same holds true in a guard-interval-assisted orthogonal frequency-division multiplexing FTNS scenario.

Most recently, in [17], the frequency-domain equalization (FDE) technique [18] that was originally developed for single-carrier frequency-division multiplexing access was applied to an uncoded hard-decision-based FTNS receiver for the first time. Owing to the explicit benefit of efficient fast Fourier transform (FFT)-based reception, this FDE receiver allows us to handle CIR spreading over thousands of symbols, while maintaining a realistic equalization complexity at the receiver. Unfortunately, this uncoded FDE-aided FTNS receiver fails to approach the optimal ML performance.

Against this background, the novel contributions of this paper are as follows.

1) Motivated by both the limitations and benefits of the recent FDE-aided hard-decision FTNS algorithm [17], we conceive a

low-complexity FDE-aided SoD demodulator for the FTNS receiver, which allows us to eliminate the ISI imposed by FTNS. The proposed scheme's low complexity is retained even in long-CIR scenarios.

2) Furthermore, we propose an advanced three-stage-concatenated FTNS transceiver, which is capable of attaining an infinitesimally low BER at a signal-to-noise ratio (SNR) close to the capacity bound.
3) Finally, we determine the maximum achievable rate, which is calculated based on EXIT charts.[2]

The remainder of this paper is organized as follows. In Section II, we detail our FTNS model and then introduce our three-stage-concatenated transceiver structure. Section III highlights our EXIT-chart-aided analysis and optimization, whereas the achievable error-rate performance is investigated in Section IV. Finally, we conclude in Section V.

II. System Model

Here, we first detail the system model of our cyclic prefix (CP)-assisted FTNS scheme, and then, the SoD FDE-aided demodulator is proposed. Finally, our serially concatenated three-stage FDE-aided FTNS transceiver structure is presented.

A. *FTNS Modulation*

Consider that a B-bit information sequence $\mathbf{b} = [b_1, \ldots, b_B] \in \mathbb{Z}^B$ is first mapped to N complex-valued symbols $\mathbf{s} = [s_1, \ldots, s_N]^T \in \mathbb{C}^N$. Then, a 2ν-sample CP $\mathbf{s}_{\mathrm{cp}} = [s_1, \ldots, s_{2\nu}]^T \in \mathbb{C}^{2\nu}$ is concatenated to the original symbol sequence $\mathbf{s}$ to construct $\bar{\mathbf{s}} = [\bar{s}_1, \ldots, \bar{s}_{N+2\nu}]^T = [\mathbf{s}^T, \mathbf{s}_{\mathrm{cp}}^T]^T \in \mathbb{C}^{N+2\nu}$. Finally, after each symbol has been convolved with the shaping pulse $h(t)$, the CP is inserted, and then, the signal is transmitted from a single transmit antenna using the symbol interval $T \leq T_0$.

At the receiver, the corresponding continuous-time received signals, which are matched-filtered by $h(t)$, are represented by

$$y(t) = \sum_n \bar{s}_n g(t - nT) + \eta(t) \tag{1}$$

where we have $g(t) = \int h(\tau) h^*(\tau - t) d\tau$ and $\eta(\tau) = \int n(\tau) h^*(\tau - t) d\tau$. Here, we assumed that an RRC filter having the roll-off factor β represents $h(t)$. Furthermore, $n(t)$ represents a random variable that obeys the zero-mean complex-valued Gaussian distribution $\mathcal{CN}(0, N_0)$, where N_0 is the noise variance. Under the perfect-synchronization assumption between the transmitter and the receiver, the kth sample is expressed as

$$\begin{aligned} \bar{y}_k &= y(kT) &(2)\\ &= \sum_n \bar{s}_n g(kT - nT) + \eta(kT). &(3) \end{aligned}$$

Furthermore, upon removing the first and the last ν samples from $\bar{y} = [\bar{y}_1, \ldots, \bar{y}_{N+2\nu}]^T$, we arrive at the frequency-domain signal represented by [17]

$$\begin{aligned} \mathbf{y} &= [\bar{y}_1, \ldots, \bar{y}_N]^T \in \mathbb{C}^N &(4)\\ &= \mathbf{G}\mathbf{s} + \mathbf{n} &(5) \end{aligned}$$

where $\mathbf{G}$ is a cyclic matrix, having the tap coefficient vector $\mathbf{g} = [g(-\nu T), \ldots, g(0), \ldots, g(\nu T)]^T \in \mathbb{R}^{2\nu+1}$, whereas $\mathbf{n}$ denotes the associated noise components. Note that similar to the assumption employed in [16], we consider the square norm $\|\mathbf{g}\|^2 = \mathbf{g}^H \mathbf{g}$ to be normalized to unity to ensure that the average received power per symbol be maintained at unity.

Here, it is assumed in (5) that the FTNS system's ISI tap length L_{FTN} in the AWGN channel is lower than the CP length ν and that other ISI components are truncated in this model. Note that in most of the previous FTNS studies, a similar truncation of high-tap terms is utilized. The exclusive benefit of our FDE-based approach is that the employment of a sufficiently high transmit-block length N makes the relative CP overhead $2\nu/N$ negligible.

B. *SoD FDE-Based FTNS Detection*

Let us now introduce the FDE-aided SoD FTNS demodulator, while assuming that BPSK modulation is employed for the sake of simplicity and of space economy. However, the extension to other nonbinary multilevel modulation schemes is readily applicable, similar to [4].

First, according to the soft-interference cancelation principle [21], the received signals are modified to

$$\begin{aligned} \tilde{\mathbf{y}} &= \mathbf{y} - \mathbf{G}\tilde{\mathbf{s}} &(6)\\ &= \mathbf{G}(\mathbf{s} - \tilde{\mathbf{s}}) + \mathbf{n} &(7) \end{aligned}$$

where the soft symbols $\tilde{\mathbf{s}} = [\tilde{s}_1, \ldots, \tilde{s}_N]^T \in \mathbb{C}^N$ are generated from the *a priori* information, which is fed back from the outer decoder. Recalling that $\mathbf{G}$ is a circulant matrix, we can rely on FFT-assisted eigenvalue decomposition, which is formulated by [17]

$$\mathbf{G} = \mathbf{Q}^T \mathbf{\Lambda} \mathbf{Q}^* \tag{8}$$

where $\mathbf{Q}$ is the Fourier matrix defined by $[\mathbf{Q}]_{k.l} = (1/\sqrt{N}) \exp[-2\pi j(k-1)(l-1)/N]$. Furthermore, $\mathbf{\Lambda}$ is the diagonal matrix, whose ith element λ_i is the associated FFT coefficient. Hence, by carrying out the FFT operation on both sides of (7), we arrive at

$$\begin{aligned} \tilde{\mathbf{y}}_f &= [\tilde{y}_{f,1}, \ldots, \tilde{y}_{f,N}]^T &(9)\\ &= \mathbf{Q}^* \tilde{\mathbf{y}} &(10)\\ &= \mathbf{\Lambda}\mathbf{Q}^*(\mathbf{s} - \tilde{\mathbf{s}}) + \mathbf{n}_f \in \mathbb{C}^N &(11) \end{aligned}$$

where $\mathbf{n}_f = \mathbf{Q}^* \mathbf{n}$ is the associated noise vector.

With the aid of minimum mean square error (MMSE) filtering, the frequency-domain symbol estimates $\hat{\mathbf{s}}_f = [\hat{s}_{f,1}, \ldots, \hat{s}_{f,N}]^T \in \mathbb{C}^N$ are given by [22]

$$\hat{s}_{f,n} = \frac{\lambda_i^*}{|\lambda_n|^2 D + N_0} \tilde{y}_{f,n} \tag{12}$$

where we have

$$D = -\sum_{i=1}^{N} |\tilde{s}_i|^2 / N. \tag{13}$$

Finally, the time-domain extrinsic log-likelihood ratio (LLR) outputs of the proposed demodulator are formulated as follows [23]:

$$\begin{aligned} \mathbf{L}_{\mathrm{e}} &= [L_{\mathrm{e}}(b_1), \ldots, L_{\mathrm{e}}(b_N)]^T &(14)\\ &= \frac{\gamma \tilde{\mathbf{s}} + \mathbf{Q}^T \hat{\mathbf{s}_f}}{1 + \gamma\delta} \in \mathbb{R}^N &(15) \end{aligned}$$

[2]To elaborate a little further, the maximum achievable rate represents the maximum practically attainable rate that takes into account the effects of a specific inner code, modulation and detection scheme, unlike the classic capacity bound. Hence, it is possible to appropriately characterize the proposed reduced-complexity SoD detector. For a detailed discussion, please refer to [19] and [20].

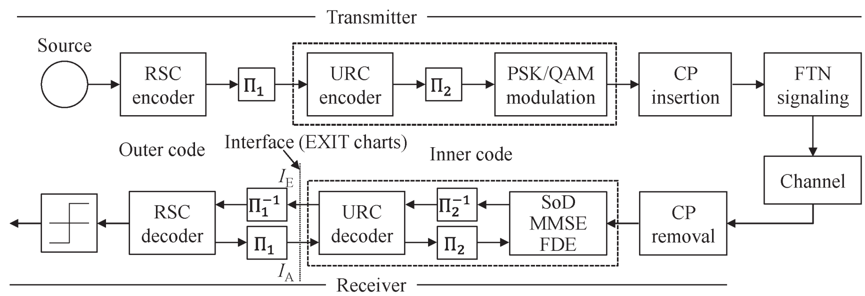

Fig. 1. Transmitter and receiver structures of our FTNS-based three-stage serially concatenated system.

where

$$\gamma = \Re\left[\sum_{i=1}^{N} \frac{|\lambda_i|^2/\left(|\lambda_i|^2 D + N_0\right)}{N}\right] \tag{16}$$

$$\delta = 1 - D. \tag{17}$$

Although in the derivation of our SoD FDE-aided FTNS demodulator we assumed having an AWGN channel, the proposed SoD demodulator is readily applicable to either frequency-flat or frequency-selective fading scenarios, provided that we set the CP size sufficiently high, as shown in [17].

C. Extension to the Frequency-Selective Fading System Model

Having introduced our FTNS transceiver model under a simplified AWGN channel assumption, let us now consider its extension to a model applicable to frequency-selective fading environments. Let us consider that the delay spread associated with frequency-selective channels spans over $L_{\mathrm{DS}}T(=\alpha L_{\mathrm{DS}}T_0)$ symbol durations and that the L_{DS} complex-valued tap coefficients are given by q_l $(l = 0, \ldots, L_{\mathrm{DS}} - 1)$. Then, by defining the first term of (3) as

$$\bar{y}_k = \sum_{n=-\nu}^{\nu} \bar{s}_n g(kT - nT) \tag{18}$$

the received signal may be expressed as

$$y_k = \sum_{l=0}^{L_{\mathrm{DS}}-1} q_l \bar{y}_{k-l} + \eta(kT) \tag{19}$$

$$= \sqrt{E_s} \sum_{l=0}^{L_{\mathrm{DS}}-1} \sum_{n=-\nu}^{\nu} s_n q_l g\left(kT - (l+n)T\right) + \eta(kT). \tag{20}$$

This system model also represents a circular-matrix-based linear block structure in the same manner as $\mathbf{G}$ of (5), where the CP length of 2ν is designed to be sufficiently higher than the effective ISI duration. Therefore, the FDE-aided FTNS technique derived in Section II-B is also readily applicable in this frequency-selective scenario.

Note that the effective ISI length in the frequency-selective scenario is a factor $(L_{\mathrm{DS}} - 1)$ higher than that considered for its frequency-flat FTNS counterpart in Section II-B. Furthermore, when we compare the effective CIR length of the FTNS- and Nyquist-sampled scenarios, the ratio becomes

$$\theta = \frac{L_{\mathrm{DS}} + L_{\mathrm{FTN}}}{\alpha L_{\mathrm{DS}}} \tag{21}$$

implying that a lower α value corresponds to a wider gap between the two. Naturally, this typically increases the detection complexity; hence, the advantage of the proposed low-complexity FDE-aided FTNS receiver over its conventional time-domain counterpart becomes further improved in this practical scenario.

D. Three-Stage-Concatenated FTNS System

Having introduced the SoD FDE-aided FTNS demodulator in Section II-B, we further improve it with the aid of a multistage serially concatenated turbo FTNS architecture, to achieve a near-capacity performance, while eliminating the limitations of ISI. More specifically, we propose the three-stage-concatenated recursive systematic convolutional (RSC)-encoded and unity-rate convolutional (URC)-encoded transmitter structure in Fig. 1. At the transmitter, the information bits are first encoded by the RSC encoder, and then, the encoded bits are interleaved by the first interleaver Π_1. Next, the interleaved bits are URC-encoded and then interleaved again by the second interleaver Π_2. Finally, the interleaved bits are mapped by the CP-assisted low-complexity FTNS modulator described in Section II-A, to construct the $(N + 2\nu)$-symbol sequence to be transmitted.

As shown in Fig. 1, a three-stage iterative decoding algorithm is employed at the receiver. To be specific, the SoD decoders of the receiver iteratively exchange soft extrinsic information in the form of LLRs. The SoD MMSE FDE block in Fig. 1 receives its input signals after CP removal, which are combined with the extrinsic information provided by the URC decoder. Simultaneously, the URC decoder block in Fig. 1 receives extrinsic information from both the RSC channel decoder and the SoD MMSE FDE demodulator and generates extrinsic information for both of its surrounding blocks, as shown in Fig. 1. The RSC channel decoder in Fig. 1 exchanges extrinsic information with the URC decoder and outputs the estimated bits after I_{out} iterations. Here, the iterations between the SoD MMSE FDE and URC decoder blocks are referred to as the inner iterations, whereas those between the URC and RSC decoders are referred to as outer iterations. The number of these iterations is represented by I_{in} and I_{out}, respectively. To be more specific, I_{in} inner iterations are implemented per each outer iteration, indicating that the total number of iterations is $I_{\mathrm{in}} \cdot I_{\mathrm{out}}$. Hence, when fixing the number of inner iterations I_{in}, it becomes possible to rely on the 2-D projection of the associated 3-D EXIT charts [19].[3]

[3]To exactly estimate the convergence behavior of our three-stage-concatenated iterative receiver, ideally, 3-D EXIT charts [24] would be used. However, they impose high analysis complexity. By contrast, the projection to 2-D EXIT charts allows us to efficiently analyze the associated iterative behavior, when the number of inner iterations I_{in} is sufficiently high for approaching the highest possible mutual information between the inner blocks [19]. Furthermore, this makes it easier to compare the iterative behaviors of the two-stage- and three-stage-concatenated iterative receivers, as demonstrated in Section III.

III. EXIT-Chart-Aided Optimization

Here, we analyze the convergence behavior of our multistage-concatenated FTNS systems. Here, we invoke EXIT charts for characterizing the FTNS scheme's near-capacity code design and the information-theoretic analysis of the maximum achievable rate.

A. Semianalytical Evaluations of Maximum Achievable Rate

In turbo detection, an infinitesimally low BER may be attained by the iterative exchange of extrinsic mutual information between multiple SoD decoders. Since the iterative decoding process is nonlinear, the prediction of its convergence behavior is a challenging task. The ingenious tool of EXIT charts was proposed by ten Brink [12] for both the visualization of the iterative decoding behavior and for the prediction of the "BER-cliff"-SNR position, where the BER suddenly drops. More specifically, the input/output relationship of the mutual information at each decoder is characterized by the EXIT chart, and then, their interaction assisted by the iterative decoding process is examined without time-consuming bit-by-bit Monte Carlo simulations.

The explicit benefit of utilizing EXIT charts for the analysis of FTNS is the capability of evaluating arbitrary detectors, including suboptimal detectors. As previously mentioned, the SoD maximum *a posteriori* (MAP) detection, which has been typically considered for the conventional channel-encoded FTNS scheme, exhibits excessive decoding complexity. Furthermore, deriving the exact performance bound of a suboptimal FTNS detector is a challenging task.

By exploiting the EXIT chart's area property detailed in [19], let us define the maximum achievable rate of our FDE-aided FTNS system as

$$\mathcal{C}_{\mathrm{EXIT}} = \frac{N}{N+2\nu} \cdot \frac{\log_2 \mathcal{M}}{\alpha(1+\beta)} \cdot \mathcal{A}(\rho) \tag{22}$$

where $\mathcal{A}(\rho)$ represents the area under the inner code's EXIT curve at SNR $= \rho$. To be more specific, when assuming that the area under an outer code's EXIT curve is perfectly matched to that under an inner code's EXIT curve, the maximum achievable rate of a serially concatenated scheme may be approximated by evaluating the area under the EXIT curves, as detailed in [19] and [25]. Exploiting this EXIT-chart-based limit allows us to evaluate the maximum attainable rate of an arbitrary iterative FTNS detection algorithm.

B. EXIT-Chart-Based Analysis of FTNS

Here, we investigate the convergence behavior and the maximum achievable rate of some specific FTNS scenarios. Here, the input/output interface of EXIT charts was assumed to be positioned between the first interleaver Π_1 and the inner code, as shown in Fig. 1. Furthermore, in addition to our three-stage-concatenated FTNS system, we also considered its two-stage counterpart as our benchmark scheme, where the second interleaver Π_2/deinterleaver Π_2^{-1} and the URC encoder/decoder were removed from the architecture in Fig. 1. In Fig. 2, we plotted the EXIT charts of our FDE-aided two-stage FTNS system, employing BPSK modulation and the FTNS parameters of $(\alpha, \beta, \nu) = (0.6, 0.5, 10)$, where the SNR was varied from -5 to 2 dB with steps of 1 dB. We also plotted the inner code's EXIT curves associated with classic Nyquist signaling. The half-rate unit-memory RSC(2,1,2) code, having the octally represented generator polynomial of $(G_r, G) = (3, 2)$ [11], was employed for the outer code, where G_r stands for the recursive feedback polynomial and feedforward polynomial G. Further, a simple rate-one accumulator, represented by the generator polynomials (3,2) expressed in octal form, was considered for the URC precoder. Observe in Fig. 2 that regardless of the SNR value, our two-stage FDE-based FTNS system converged to that of its classic Nyquist-criterion-based counterpart for $I_{\mathrm{A}} = 1.0$. Hence, it is predicted that our proposed low-complexity FDE-based algorithm is capable of achieving the same error-rate performance as that of the equivalent Nyquist-criterion-based scheme, which is an explicit benefit of the iterative receiver architecture.[4]

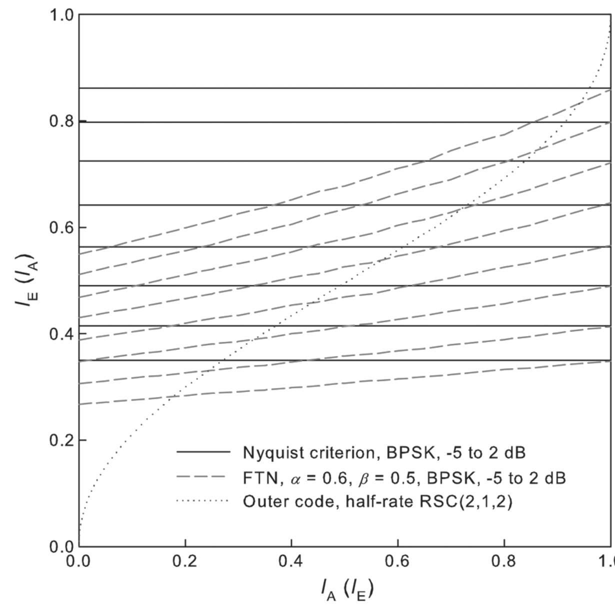

Fig. 2. EXIT charts of our FDE-aided two-stage FTNS system, employing the BPSK modulation and FTNS parameters of $(\alpha, \beta, \nu) = (0.6, 0.5, 10)$, where the SNR was varied from -5 to 2 dB with steps of 1 dB. The number of inner iterations was maintained to be $I_{\mathrm{in}} = 2$ throughout this paper. Moreover, we plotted the inner code's EXIT curves associated with the classic Nyquist-criterion scenario, while showing the outer code's EXIT curve corresponding to the half-rate RSC(2,1,2) code, having the generator polynomial of $(G_r, G) = (3, 2)$.

In Fig. 3, we drew the EXIT charts of our FDE-aided three-stage FTNS system, employing BPSK modulation and the FTNS parameters of $(\alpha, \beta, \nu) = (0.6, 0.5, 10)$, where the SNR was set to 1 dB. We also plotted the inner code's EXIT curves associated with the conventional Nyquist criterion, while showing the outer code's EXIT curve corresponding to the half-rate RSC(2,1,2) code, having the octal generator polynomials of (3,2). The transmit block length was set to $N = 2^{17}$. It can be seen in Fig. 3 that our three-stage FTNS scheme approached the point $(I_{\mathrm{A}}, I_{\mathrm{E}}) = (1.0, 1.0)$ of perfect convergence to an infinitesimally low BER. This was achieved as the explicit benefit of the URC precoder, which creates an infinite impulse response inner decoder component [27] and [28] to reach the $(I_{\mathrm{A}}, I_{\mathrm{E}}) = (1, 1)$ point of convergence in the EXIT chart, hence achieving an infinitesimally low BER.

This was also confirmed by the Monte-Carlo-simulation-based EXIT trajectory shown in Fig. 3.

Furthermore, in Fig. 4, we plotted the EXIT charts of our three-stage-concatenated FDE-aided FTNS systems, where the roll-off factor β was given by (a) 0.1, (b) 0.5, while maintaining the symbol's packing ratio of $\alpha = 0.6$. The SNR of the outer code's EXIT curve was varied from -10 to 10 dB with steps of 1 dB. It can be seen in Fig. 4 that at high SNRs, a higher-β inner-code EXIT curve corresponds to

[4] To provide further insights, this inner code's convergence to that of its interference-free Nyquist-criterion-based counterpart can also be seen in rank-deficient spatial-multiplexing MIMO scenarios [26], where the number of receive antenna elements is lower than that of the transmit antenna elements.

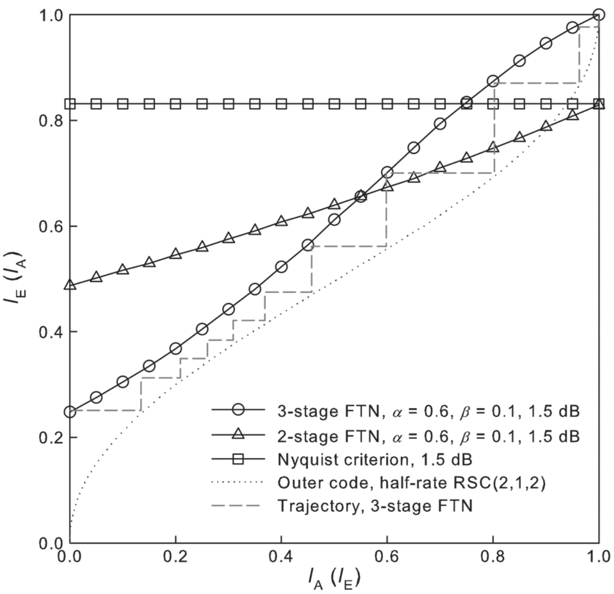

Fig. 3. EXIT charts of our FDE-aided three-stage FTNS system, employing BPSK modulation and the FTNS parameters of $(\alpha, \beta, \nu) = (0.6, 0.5, 10)$, where the SNR was set to 1 dB. Moreover, we plotted the inner code's EXIT curves associated with the classic Nyquist-criterion scenario, while showing the outer code's EXIT curve corresponding to the half-rate RSC(2,1,2) code, which has the generator polynomial (3,2). The code length was set to $N = 2^{17}$.

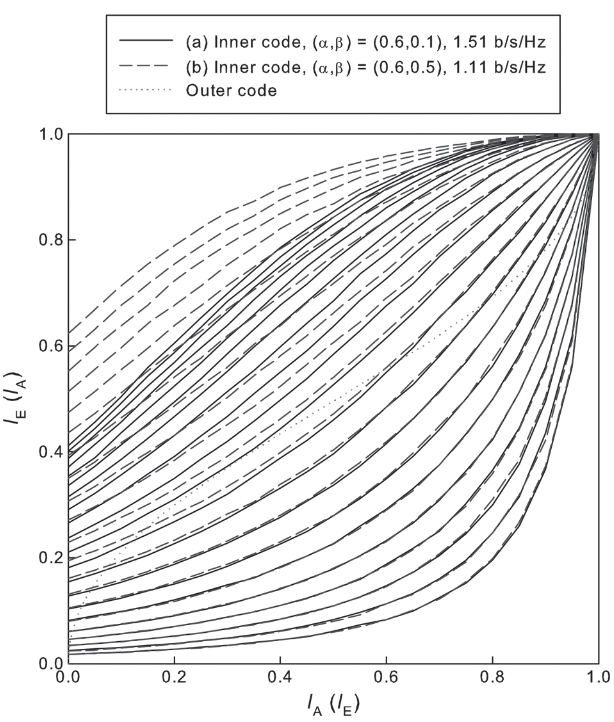

Fig. 4. EXIT charts of our three-stage-concatenated FDE-aided FTNS systems, where the roll-off factor β was given by (a) 0.1, (b) 0.5, while maintaining the symbol's packing ratio $\alpha = 0.6$. The SNR of the outer code's EXIT curve was varied from -10 to 10 dB with steps of 1 dB.

a higher performance, i.e., to a wider open-tunnel area between the inner and outer codes' EXIT curves. However, regardless of the roll-off factor value β, an open EXIT tunnel emerged at SNR ≥ 1 dB; therefore, affording an increased number of iterations enabled us to attain a higher transmission rate without imposing any SNR penalty,

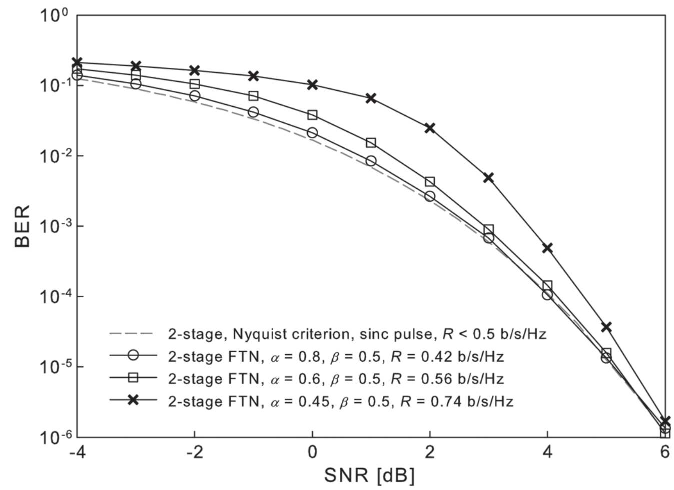

Fig. 5. Achievable BER of our FDE-aided two-stage RSC-encoded FTNS systems, employing BPSK modulation and FTNS parameters of $(\alpha, \beta, \nu) = (0.45, 0.5, 10)$, $(0.6, 0.5, 10)$, and $(0.8, 0.5, 10)$. Moreover, we plotted the BER curve of the conventional Nyquist-criterion scenario as a benchmark scheme. The half-rate RSC(2,1,2) code, having the polynomial generator of (3,2) and the code length $N = 2^{17}$, was considered.

which is particularly beneficial for our FTNS receiver exhibiting low detection complexity.[5]

As previously mentioned, nonbinary multilevel modulation schemes may also be used for our FTNS scheme instead of a binary modulation scheme. However, in such a scenario, either the bitwise soft-input/output relationship has to be considered for the EXIT chart analysis, as shown in [23], or corresponding symbol-based EXIT charts have to be used.

IV. Error-Rate Performance Results

To further characterize our FDE-aided two- and three-stage-concatenated FTNS systems, we investigated their BER based on extensive Monte Carlo simulations.

First, Fig. 5 shows the achievable BER of our FDE-aided two-stage FTNS systems employing BPSK modulation and FTNS parameters of $(\alpha, \beta, \nu) = (0.45, 0.5, 10)$, (0.6, 0.5, 10), and (0.8, 0.5, 10), along with the BER of the conventional Nyquist-criterion-based scenario as a benchmarker and with the outer code's EXIT curve corresponding to the half-rate RSC(2,1,2) code, having the octal generator polynomials of (3,2). The transmit block length was set to $N = 2^{17}$. In this simulation scenario, our FTNS scheme's transmission rate was varied from 0.42 to 0.74 b/s/Hz, while, at the same time, the symbol packing coefficient α was decreased from 0.8 to 0.45. Observe in Fig. 5 that the two-stage iterative detection converged to the ISI-free Nyquist-criterion-based curve upon increasing SNR. This was achieved regardless of the symbol packing ratio α. More specifically, this configured the EXIT chart analysis conducted in Fig. 2. Observe that our reduced-complexity FDE receiver was found to perfectly eliminate the ISI effects, similar to its time-domain SoD MAP counterparts characterized [6] and [1].

In Fig. 6, we compared the achievable BER curves of our FDE-aided two- and three-stage FTNS systems employing BPSK modulation and

[5] In the simulations, we only considered the half-rate RSC(2,1,2) code as our outer code. However, it may be possible to employ other types of outer codes, which potentially attains a better match between the outer and inner codes' EXIT curves. For example, irregular channel codes [19] and [24] are capable of flexibly designing an outer code's EXIT curve, which matches the inner code's EXIT curve at a given SNR.

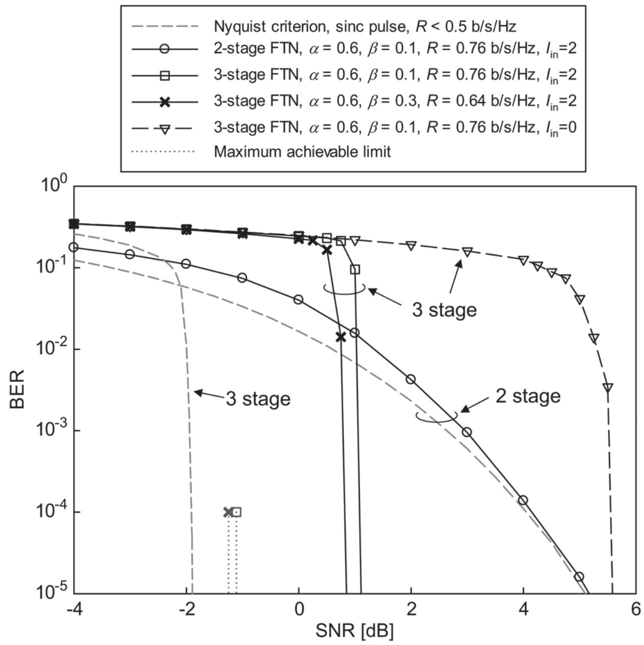

Fig. 6. Achievable BER of our FDE-aided two- and three-stage FTNS systems, employing BPSK modulation and FTNS parameter sets of $(\alpha, \beta, \nu) = (0.6, 0.1, 10)$ and $(0.6, 0.3, 10)$. Moreover, we plotted the BER of the conventional Nyquist-criterion scenario. Here, we assumed the employment of the half-rate RSC(2,1,2) code, which has the polynomial generator (3,2) and a code length $N = 2^{17}$.

the FTNS parameter sets of $(\alpha, \beta, \nu) = (0.6, 0.1, 10)$ and (0.6, 0.3, 10). We also plotted the two BER curves associated with the conventional Nyquist-criterion-based scenario. Moreover, we plotted the associated BER curve of the FDE-aided three-stage FTNS system that dispenses with inner iterations, i.e., for $I_{\rm in} = 0$, to explicitly clarify the beneficial effects of the *a priori* information fed back to our SoD FDE. Here, we assumed the employment of the half-rate RSC(2,1,2) code, having the octal generator polynomials of (3,2), and the block length was set to $N = 2^{17}$. It was found in Fig. 6 that both the proposed three-stage systems having $\beta = 0.1$ and 0.3 exhibited an infinitesimally low BER at SNR $= 1.0$ and 1.3 dB, respectively, whereas its two-stage counterpart did not. More specifically, these BER cliffs were apart by as little as 2.1 and 2.5 dB from the maximum achievable limits, which were calculated based on the EXIT chart analysis in Fig. 3. Note that the BER curves of the Nyquist-criterion-based systems were calculated under the idealistic assumption of sinc-pulse transmissions, which cannot be used in a practical system. Additionally, the transmission rate was lower than that of the FTNS systems. Moreover, the three-stage FTNS system dispensing with inner iterations ($I_{\rm in} = 0$) imposed more than 4-dB performance penalty in comparison to that having $I_{\rm in} = 2$ inner iterations. Therefore, the joint optimization of the three SoD decoders is quite crucial for the sake of ensuring the most appropriate extrinsic-information exchange.

Finally, in Fig. 7, we plotted the BER curves of our three-stage-concatenated FTNS systems having the CP length of $2\nu = 32$, 36, 40, and 48, when using a constant block length of 512 bits, while considering frequency-selective block Rayleigh fading. Furthermore, the interleaver length of 2^{17} and the FTNS parameter set of $(\alpha, \beta) = (0.6, 0.1)$ were employed. The delay spread was set to $L_{\rm DS} = 20$. Furthermore, the fading coefficients q_l $(l = 0, \ldots, L_{\rm DS})$ were randomly generated according to the complex-valued Gaussian distribution $\mathcal{CN}(0,1/L_{\rm DS})$. Observe in Fig. 7 that upon increasing the CP length, the error floor caused by the FTNS-induced ISI and by the

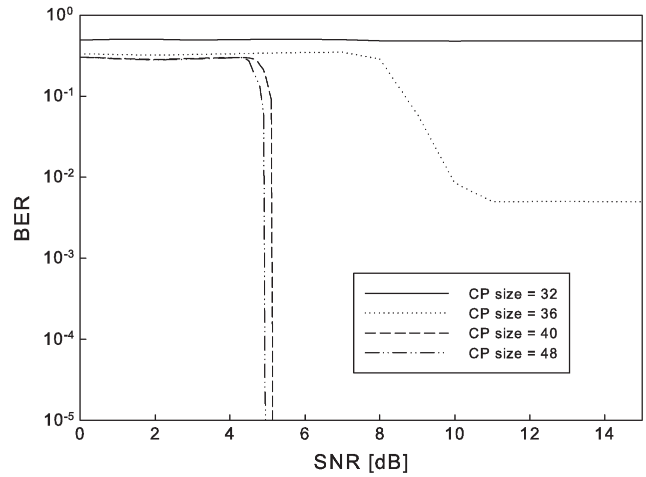

Fig. 7. Achievable BER of our FDE-aided three-stage FTNS systems, experiencing frequency-selective block Rayleigh fading, where we considered the delay spread of $L_{\rm DS} = 20$ taps. The BPSK modulation and the FTNS parameter set of $(\alpha, \beta) = (0.6, 0.1)$ were employed, while varying the CP length 2ν from 32 to 48. Here, we assumed the employment of the half-rate RSC(2,1,2) code, which has the polynomial generator (3,2) and a code length $N = 2^{17}$.

long-CIR dispersive channel was eliminated. More specifically, it was found that to compensate the ISI, a CP length of $2\nu \geq 40$ was required in this specific simulation scenario. This implies that the conventional TDE-based FTNS receivers are incapable of supporting such a long CIR owing to their prohibitively high decoding complexity.

V. Conclusion

In this paper, we have proposed a novel reduced-complexity SoD FTNS receiver structure for long-CIR gigabit systems, which relied on the FDE principle. The proposed detector is capable of eliminating FTNS-specific ISI, while maintaining practical decoding complexity. Furthermore, we carried out its comprehensive EXIT-chart-aided analysis to design a near-capacity three-stage serially concatenated FTNS architecture, which is free from an error floor. Our simulation results demonstrated that the proposed FTNS scheme has the explicit benefits of lower complexity and better BER performance than those of its conventional channel-encoded FTNS counterpart.

References

[1] J. B. Anderson, F. Rusek, and V. Owall, “Faster than Nyquist signaling,” *Proc. IEEE*, vol. 101, no. 8, pp. 1817–1830, Aug. 2013.
[2] J. E. Mazo, “Faster-than-Nyquist signaling,” *Bell Syst. Tech. J.*, vol. 54, no. 8, pp. 1451–1462, Oct. 1975.
[3] J. Esch, “Prolog to faster-than-Nyquist signaling,” *Proc. IEEE*, vol. 101, no. 8, pp. 1815–1816, Aug. 2013.
[4] F. Rusek and J. B. Anderson, “Non binary and precoded faster than Nyquist signaling,” *IEEE Trans. Commun.*, vol. 56, no. 5, pp. 808–817, May 2008.
[5] F. Rusek, “On the existence of the Mazo-limit on MIMO channels,” *IEEE Trans. Wireless Commun.*, vol. 8, no. 3, pp. 1118–1121, Mar. 2009.
[6] A. D. Liveris and C. N. Georghiades, “Exploiting faster-than-Nyquist signaling,” *IEEE Trans. Comm.*, vol. 51, no. 9, pp. 1502–1511, Sep. 2003.
[7] G. Colavolpe, T. Foggi, A. Modenini, and A. Piemontese, “Faster-than-Nyquist and beyond: How to improve spectral efficiency by accepting interference,” *Opt. Exp.*, vol. 19, no. 27, pp. 26 600–26 609, Dec. 2011.
[8] S. Liu and Z. Tian, “Near-optimum soft decision equalization for frequency selective MIMO channels,” *IEEE Trans. Signal Process.*, vol. 52, no. 3, pp. 721–733, Mar. 2004.
[9] S. Sugiura, S. Chen, and L. Hanzo, “MIMO-aided near-capacity turbo transceivers: Taxonomy and performance versus complexity,” *IEEE Commun. Surveys Tuts.*, vol. 14, no. 2, pp. 421–442, 2012.

[10] F. Rusek and J. Anderson, "Multistream faster than Nyquist signaling," *IEEE Trans. Commun.*, vol. 57, no. 5, pp. 1329–1340, May 2009.

[11] S. ten Brink, "Designing iterative decoding schemes with the extrinsic information transfer chart," *AEU Int. J. Electron. Commun.*, vol. 54, no. 6, pp. 389–398, Nov. 2000.

[12] S. ten Brink, "Convergence behavior of iteratively decoded parallel concatenated codes," *IEEE Trans. Commun.*, vol. 49, no. 10, pp. 1727–1737, Oct. 2001.

[13] A. Prlja, J. B. Anderson, and F. Rusek, "Receivers for faster-than-Nyquist signaling with and without turbo equalization," in *Proc. IEEE Int. Symp. Inf. Theory*, Toronto, Canada, Jul. 6–11, 2008, pp. 464–468.

[14] M. McGuire and M. Sima, "Discrete time faster-than-Nyquist signalling," in *Proc. IEEE Global Telecommun. Conf.*, 2010, pp. 1–5.

[15] J. B. Anderson and M. Zeinali, "Best rate 1/2 convolutional codes for turbo equalization with severe ISI," in *Proc. IEEE ISIT*, 2012, pp. 2366–2370.

[16] A. Prlja and J. B. Anderson, "Reduced-complexity receivers for strongly narrowband intersymbol interference introduced by faster-than-Nyquist signaling," *IEEE Trans. Commun.*, vol. 60, no. 9, pp. 2591–2601, Sep. 2012.

[17] S. Sugiura, "Frequency-domain equalization of faster-than-Nyquist signaling," *IEEE Wireless Commun. Lett.*, vol. 2, no. 5, pp. 555–558, Oct. 2013.

[18] D. Falconer, S. Ariyavisitakul, A. Benyamin-Seeyar, and B. Eidson, "Frequency domain equalization for single-carrier broadband wireless systems," *IEEE Commun. Mag.*, vol. 40, no. 4, pp. 58–66, Apr. 2002.

[19] L. Hanzo, O. Alamri, M. El-Hajjar, and N. Wu, *Near-Capacity Multi-Functional MIMO Systems: Sphere-Packing, Iterative Detection and Cooperation*. Hoboken, NJ, USA: Wiley, 2009.

[20] M. El-Hajjar and L. Hanzo, "EXIT charts for system design and analysis," *IEEE Commun. Surveys Tuts.*, vol. 16, no. 1, pp. 127–153, 2014, early access in IEEE Xplore.

[21] M. Tüchler, A. Singer, and R. Koetter, "Minimum mean squared error equalization using *a priori* information," *IEEE Trans. Signal Process.*, vol. 50, no. 3, pp. 673–683, Mar. 2002.

[22] B. Ng, C.-T. Lam, and D. Falconer, "Turbo frequency domain equalization for single-carrier broadband wireless systems," *IEEE Trans. Wireless Commun.*, vol. 6, no. 2, pp. 759–767, Feb. 2007.

[23] K. Kansanen and T. Matsumoto, "An analytical method for MMSE MIMO turbo equalizer EXIT chart computation," *IEEE Trans. Wireless Commun.*, vol. 6, no. 1, pp. 59–63, Jan. 2007.

[24] F. Brännström, L. K. Rasmussen, and A. J. Grant, "Convergence analysis and optimal scheduling for multiple concatenated codes," *IEEE Trans. Inf. Theory*, vol. 51, no. 9, pp. 3354–3364, Sep. 2005.

[25] A. Ashikhmin, G. Kramer, and S. Ten Brink, "Extrinsic information transfer functions: Model and erasure channel properties," *IEEE Trans. Inf. Theory*, vol. 50, no. 11, pp. 2657–2673, Nov. 2004.

[26] L. Xu, S. Chen, and L. Hanzo, "EXIT chart analysis aided turbo MUD designs for the rank-deficient multiple antenna assisted OFDM uplink," *IEEE Trans. Wireless Communications*, vol. 7, no. 6, pp. 2039–2044, Jun. 2008.

[27] S. Benedetto, D. Divsalar, G. Montorsi, and F. Pollara, "Serial concatenation of interleaved codes: Performance analysis, design, iterative decoding," *IEEE Trans. Inf. Theory*, vol. 44, no. 3, pp. 909–926, May 1998.

[28] F. Schreckenbach and G. Bauch, "Bit-interleaved coded irregular modulation," *Eur. Trans. Telecommun.*, vol. 17, no. 2, pp. 269–282, Mar./Apr. 2006.

AUTHOR QUERIES

AUTHOR PLEASE ANSWER ALL QUERIES

AQ1 = Please provide the expanded forms of “JST-ASTEP” and “KAKENHI” if such are acronyms.

END OF ALL QUERIES